Membrane and Water Treatment, *Vol. 16, No. 3 (2025) 121-132*
https://doi.org/10.12989/mwt.2025.16.3.121

Thin film nanocomposite (TFN) membranes filled with a novel metal organic framework for reverse osmosis applications

Mohammed Kadhom*[1], Noor Albayati[2], Alaa E. Sultan[3], Mudhar A. Al-Obaidi[4], Suhaib Salih[5] and Baolin Deng**[6]

[1]*Department of Environmental Science, College of Energy and Environmental Science, Alkarkh University of Science, Baghdad, 10081, Iraq*
[2]*Department of Chemical Engineering, College of Engineering, University of Baghdad, Baghdad, 10071, Iraq*
[3]*Department of Chemistry, College of Science, University of Diyala, Baquba, 32001, Diyala, Iraq*
[4]*Technical Institute of Baquba, Middle Technical University, Baquba, Diyala, 32001, Iraq*
[5]*Department of Chemical Engineering, College of Engineering, Tikrit University, Tikrit, Saladin, 34001, Iraq*
[6]*Department of Civil and Environmental Engineering, College of Engineering, University of Missouri-Columbia, Columbia, MO, 65211, United States*

(Received September 24, 2024, Revised December 15, 2024, Accepted December 19, 2024)

Abstract. This paper reports the synthesis and use of a novel metal-organic framework (MOF), named Zr-BADS, within the thin-film nanocomposite (TFN) membranes for reverse osmosis (RO) applications. Two types of zirconium-based MOFs, Zr-BADS-1 and Zr-BADS-2, were synthesized via a solvothermal method using bicinchoninic acid disodium salt as a linker and either dimethylformamide or ethanol as solvent, respectively. TFN membranes were prepared by embedding these MOFs within the polyamide thin film supported by a polysulfone support sheet. The specific surface area of Zr-BADS-1 and Zr-BADS-2 was determined to be 396.1 and 278.6 m^2/g, respectively, indicating significant surface area conducive to water permeation. Scanning electron microscopic analysis revealed a uniform distribution of Zr-BADS nanoparticles (NPs) with particle sizes ≤ 100 nm within the TFN membranes. TEM images confirmed the dense packing of NPs within the membranes, influencing their texture and enhancing performance. FTIR spectroscopy demonstrated the presence of characteristic peaks corresponding to MOFs within the TFN membranes, with changes observed at higher loading ratios. The observed contact angle decreased with increasing MOF loadings, indicating an enhancement in the hydrophilicity. Zr-BADS-1 NPs increased water flux at its optimal loading of 0.3%, and the flux raised to 5.4 L/m^2 h bar. Salt rejection slightly decreased at low concentrations but improved at higher loading ratios, indicating the interplay between porosity and charge effects. Zr-BADS-1 outperformed other MOFs in salt rejection and water flux, suggesting it is a remarkable RO membrane filler. This study demonstrates the potential of Zr-BADS MOFs for future membrane applications in the environment.
Keywords: desalination; MOFs; reverse osmosis; TFN membranes; water treatment

1. Introduction

In light of the exponential growth of the global population over recent decades, there has been an explicit demand for freshwater (Azeez *et al*. 2023). Different methods are applied to purify or reuse water from alternative sources, where the decision to use a specific process is dependent on the contaminant type and goal specifications (Kadhom *et al*. 2022, Sandid *et al*. 2022). Large-size pollutants, such as heavy metals (Alalwan *et al*. 2020, Salih *et al*. 2019, 2022), organics, and dyes (Kadhom *et al*. 2020, Oladoye *et al*. 2023), can be easily removed by adsorption or other techniques (Yang *et al*. 2022). However, when it comes to small-sized ions, such as sodium chloride, approaches for its removal or desalination are limited (Kadhom 2023b). Desalination of marine and brackish water is crucial for drinking, agricultural, and industrial uses (Al-Furaiji *et al*. 2020). Recently, large-scale desalination facilities have proliferated worldwide, and this trend is projected to continue (Elimelech and Phillip 2011). Due to its reliability, cost-effectiveness, and environmental friendly-ness, reverse osmosis (RO) is the favored technology for increasing desalination capacity. In recent times, numerous studies have focused on refining the RO process to reduce energy consumption (Van der Bruggen and Vandecasteele 2002).

The RO technique desalinates by employing pressure to drive water from a saline side through a semi-permeable membrane to a permeate side (Kadhom and Deng 2019a). For the system to operate, the exerted pressure must exceed the osmotic pressure of the saline solution. The selective membrane allows water molecules to pass while blocking hydrated salt ions (Hua *et al*. 2017). RO has proven to be a reliable method, even on a large scale. Since the establishment of the first RO plant nearly fifty years ago, this method rapidly gained prominence in the burgeoning desalination industry two decades later. Presently, it significantly impacts freshwater availability in various regions (Kadhom and Deng 2019b, Zhao *et al*. 2013).

*Corresponding author, Assistant Professor,
E-mail: kadhom@kus.edu.iq

**Co-corresponding author, Professor,
E-mail: dengb@missouri.edu

ISSN: 2005-8624 (Print), 2092-7037 (Online)

In the RO process, the membrane is fundamental. Its beginning was in the late 1950s when Loeb and Sourirajan created the first practical membrane composed of cellulose acetate (Kalash et al. 2020). Research and practical uses mostly concentrated on membrane development from the late 1950s to the early 1980s. John Caddote's invention of the polyamide (PA) thin film composite (TFC) membrane, however, caused the sector to change dramatically. In an organic solvent, trimesoyl chloride (TMC) and m-phenyldiamine (MPD) in an aqueous solution underwent interfacial polymerization (IP), which produced the thin film (Kadhom and Deng 2019a). With continuous work to improve its performance by employing additives, the TFC membrane has become the most sophisticated technology for RO operations. Integration of nanoparticles (NPs) of different materials, such as silica (Kalash *et al*. 2020, Li *et al*. 2024), clay (Kadhom and Deng 2019b), cellulose (Kadhom *et al*. 2019), zeolite (Zhao *et al*. 2013), and metal-organic frameworks (Kadhom *et al*. 2017, Kadhom and Deng 2018), within the membrane results in the formation of thin film nanocomposite (TFN) membranes with improved performance. Post-treatment techniques (Yin *et al*. 2012) have also been used to improve membrane quality even more. Usually a few hundred nanometers thick, the TFC membrane is fastened to a polymeric supporting sheet, such as the PSU ultrafiltration membrane prepared by phase inversion (Kadhom and Deng 2019a). Various theories, including the solution-diffusion theory, have clarified the membrane-based desalination process. This theory holds that water and salt molecules migrate through the PA layer, therefore enabling transport from one side to the other (Kadhom 2023a). Preventing biofouling and drawing water molecules depend on the great hydrophilicity of this membrane (Al-Furaiji *et al*. 2022). Assessing the development and enhancing the membrane performance call for a thorough investigation.

Metal-organic frameworks (MOFs) have drawn great interest in recent years with their fascinating chemistry and possible uses. Separation science researchers used MOFs for water treatment and gas separation (Kadhom and Deng 2018). MOFs show very large surface areas, plentiful adsorption sites, varied particle structures, unusual pore sizes, and modifiable structures. These criteria qualified the MOFs for use in several domains (Kadhom *et al*. 2023). Among these uses are ion exchange (An and Rosi 2010), light harvesting (Lee *et al*. 2011), sensing (Allendorf *et al*. 2009), catalysis (Ma *et al*. 2009), drug delivery (Della Rocca *et al*. 2011), gas storage (Murray *et al*. 2009), and separation (Kadhom *et al*. 2023, Kadhom and Deng 2018). MOFs' adaptability comes from their capacity to be readily customized for particular uses.

Because of their porous structure, which creates a great volume of pores and surface area, MOFs are often employed in gas separation (Farha *et al*. 2012). This quality makes them perfect for gas storage and separation; the first MOF membrane used for gas separation (Liu *et al*. 2009). Inclusion of MOFs particles into the polyamide layer of TFN membranes has resulted in improved characteristics for separation in the aqueous phase (Kadhom *et al*. 2017). Alumina hollow fiber membranes for water desalination use MOFs as heavy metal adsorbents and fillers (Liu *et al*. 2015). TFN membranes are also used for water treatment. For example, Lee *et al*. embedded and dissolved water-soluble MOFs such A100 and C300 into ultrafiltration membranes to boost porosity (Lee *et al*. 2014).

In a previous research from our group, UiO-66 and MIL-125 MOFs were used in the TFN membrane to enhance its desalination performance (Kadhom *et al*. 2017). Various weight ratios were used to include the roughly 100 nm NPs into the membranes. The water filtration rate was raised from 62.5 $L.m^{-2}.h^{-1}$ for the plain membrane to 74.9 $L.m^{-2}.h^{-1}$ and 85.0 $L.m^{-2}.h^{-1}$ for the TFN composite membranes at the ideal loadings of 0.15% for UiO-66 and 0.3% for MIL-125, respectively. Though the addition of MIL-125 NPs slightly improved NaCl rejection, the inclusion of UiO-66 NPs had a negligible impact. Rejection rates stayed over 98.5%. Likewise, Xiao *et al*. (2019) used UiO-66 and UiO-66-NH_2 to generate TFN membranes in the MPD or TMC solutions. Their findings showed that the TFN membrane had a high water flux of 87.86 $L.m^{-2}.h^{-1}$ by adding 0.2 w/v% UiO-66 to the organic phase, as opposed to the 46.31 $L.m^{-2}.h^{-1}$ for the membrane prepared by adding 0.3 w/v% UiO-66 in the aqueous phase. When UiO-66 was added to the organic phase, the interfacial polymerization rate remarkably dropped, which was attributed to this difference. Here, a thinner and more porous polyamide thin film layer was produced, which lowers water transmission resistance during filtration. When UiO-66-NH_2 was used, the opposite situation was observed and ascribed to the better hydrophilicity of the amino group in UiO-66-NH_2, therefore improving membrane uniformity and water dispersibility. UiO-66-NH_2 also delayed the interfacial polymerization process, resulting in a more porous membrane structure. Farahbakhsh *et al*. (2024) recently created sophisticated TFC-RO membranes utilizing dual modifications employing NH_2-MIL-125 and functionalized multiwalled carbon nanotubes (MWCNTs). The changes produced more than 97% NaCl rejection and a 70% increase in water flow. These membranes also showed outstanding antifouling qualities against nanoplastics and bovine serum albumin (BSA). Koriem *et al*. (2023) created mixed matrix membranes for reverse osmosis desalination in another related study by combining cellulose acetate (CA) and polyvinylidene fluoride (PVDF) with UiO-66 nano-MOF. With 90.2% salt rejection and a permeate water flux of 5.7 $L.m^{-2}.h^{-1}$, the optimized membrane showed a 12% and 42% improvement in salt rejection and water flux, respectively, over non-impregnated blends.

Based on the remarkable properties and performance of MOFs, our group worked on developing the already-innovated ones (Albayati and Kadhom 2020) and synthesizing others (Albayati *et al*. 2024). Recently, we reported the synthesis and properties of a novel MOF (Zr-BADS) (Albayati *et al*. 2024), which showed premium results when applied in water treatment applications. In this work, we are reporting its incorporation within the TFN membranes to improve the membrane's performance for brackish water desalination. Two preparation methods were involved to synthesize Zr-BADS depending on the used solvents, and different techniques were applied to characterize the

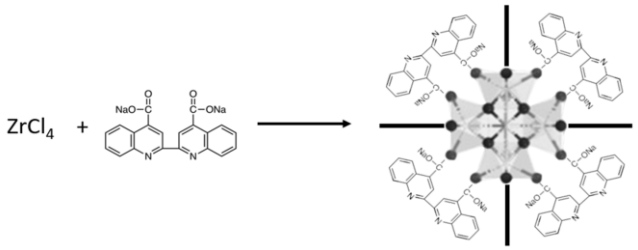

Fig. 1 The preparation reaction of Zr-BADS (Albayati *et al*. 2024)

properties and performance of the prepared membranes. Our findings in this work motivated us to utilize this material in other applications, as we will report in our coming projects.

2. Materials and methods

2.1 Chemicals

To prepare the MOFs, the following materials were obtained from Sigma-Aldrich (St. Louis, MO, USA): 4,4'-dicarboxy-2,2'-biquinoline (bicinchoninic acid) disodium salt with a water content of 2.5 mol/mol, zirconium(IV) chloride ($ZrCl_4$, 99.5%), dimethylformamide (DMF, 99.9%), and ethanol (≥ 99%). Additionally, polysulfone (PSU) pellets for the support layer and DMF were also sourced from Sigma-Aldrich. The supplier also provided (1s)-(+)-10-camphorsulfonic acid (CSA, 99%) and triethylamine (TEA, ≥ 99%) used in preparing the CSA/TEA salt. The raw materials for the IP were *m*- phenyldiamine (MPD, ≥ 99%) from Fisher Scientific (Pittsburgh, PA, USA) and trimesoyl chloride (TMC, ≥ 98.5%) from Sigma-Aldrich. Their solvents, 2,2,4- trimethylpentane (Isooctane, 99%) and DI water, were purchased from Fisher Scientific and obtained from a Millipore water system (Synergy 185, 18.2 MΩ cm), respectively. The same water system provided DI water for cleaning, casting, and other purposes. Finally, $CaCl_2$ was supplied by Fisher Scientific.

2.2 Preparation of MOFs

Zr-BADS was prepared following the protocol described in our recently published paper (Albayati *et al*. 2024). The synthesis of Zr-BADS MOF involved utilizing $ZrCl_4$ as the metallic precursor and 4,4'-dicarboxy-2,2'- biquinoline (bicinchoninic acid disodium salt) as the linker in a DMF solvent. The preparation procedure involved the solvothermal method, where the mixture was sealed in a 500 ml Teflon lined container within a metal autoclave in molar ratios of 1:1:500 for the metal: linker: solvent, respectively. The autoclave was then placed in a furnace and maintained at 120 °C for 48 h. After cooling to room temperature, the product was isolated via centrifugation, followed by methanol washing and drying at 80 °C overnight. This MOF is denoted as Zr-BADS-1. When ethanol is employed instead of the DMF at the same operational conditions, the prepared MOF is denoted as Zr-BADS-2. Fig. 1 illustrates the synthesis process and the anticipated structure of the produced MOF. Regarding the characterizations of the prepared MOF, we have reported them in our previous paper (Albayati *et al*. 2024).

2.3 Fabrication of PSU supporting layers

A casting solution was made by dissolving PSU grains, comprising 15% of the total weight, in DMF. The solution was subjected to a temperature of 60 °C and stirred for a minimum of 5 h until it achieved a colorless appearance. After being cooled to the ambient temperature and allowing any organic vapor to escape through a vent, the solution was left undisturbed overnight for degassing. The solution was equally distributed over a glass plate and transformed into a layer that was 130 µm thick using a casting knife (EQ-Se-KTQ-150, MTI Corp., Richmond, CA, USA). The glass plate containing the PSU solution was completely immersed in a water bath, resulting in swift phase inversion and the creation of a white sheet that detached from the glass surface within a few seconds. The support sheets obtained were subjected to three washes in DI water to eliminate any remaining solvents. Ultimately, the sheets were submerged in DI water at a temperature of 4 °C for a minimum of 24 h prior to usage in order to completely remove any leftover solvent.

2.4 TFN membranes preparation

To prepare the TFN membrane, initially, a PSU support layer was lifted from the water and transferred onto a glass surface, with residual water droplets removed using a squeegee roller. The PSU sheet was then immersed in an amine-based solution comprising 2% MPD, 1% CSA/TEA salt, and 0.01% $CaCl_2$ for 25 s, followed by elimination of excess MPD solution using the roller and air-drying for 2 min. Subsequently, the sheet was submerged in an organic phase containing 0.15% TMC in isooctane for 15 s to induce interfacial polymerization, resulting in the formation of a PA membrane. The choice of isooctane as the TMC solvent was based on prior research. The composite membrane underwent drying in an oven at 80°C for 6 min and was then rinsed with DI water to remove residual solutions. Initial membrane sheets were immersed in deionized water at 4 °C for at least 20 h before testing. Additionally, the nanocomposite with Zr-BADS was prepared by adding varying weight ratios of the MOF ranging from 0.05-0.4% and 0.05-0.5% for the Zr-BADS-1 and Zr-BADS-2, respectively. These particles were added to the TMC solution, ensuring proper dispersion through sonication for 30 min.

2.5 Assessments of MOFs and TFN membrane properties

The N_2-adsorption technique was employed to determine the specific surface area of Zr-BADS. The measurement was conducted using the Beckman Coulter SA 3100 surface area analyzer, manufactured by Beckman Coulter, Inc. in Brea, CA, USA. The study was performed using the Brunauer-Emmett-Teller (BET) technique. Following a drying period of roughly 24 h at room temperature and

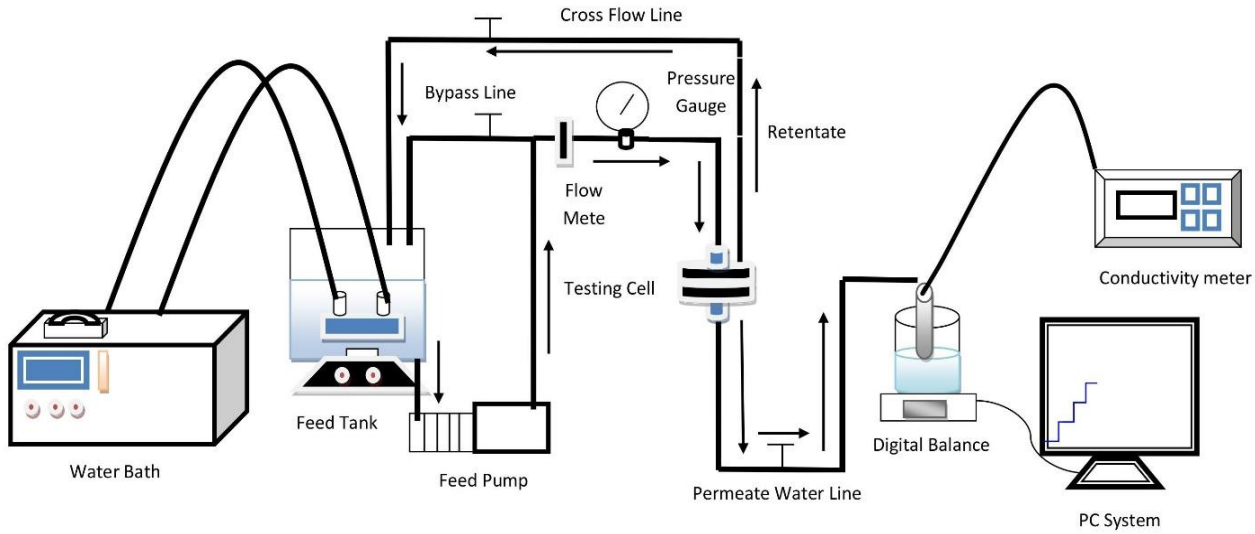

Scheme 1 A diagram of the RO operation system used to examine the membrane (Kadhom and Deng 2019b)

subsequent storage at 4 °C, the TFN membranes were subjected to further examination. The zeta potential was performed using a zeta potential device from Brookhaven Instruments Corporation (Nashua, NH, USA). The morphology of the membranes was analyzed utilizing a Hitachi S-4700 scanning electron microscope (SEM). The specimens underwent platinum coating using a sputter coater (Emitech, K575x) for 1 minute at a current intensity of 20 milliAmps. After being inserted into the SEM equipment, a variety of voltages were employed to attain different resolutions for analysis.

The cross-sectional image of the membrane was studied using the TEM apparatus (JEOL JEM-1400, JEOL Ltd., Peabody, MA, USA). Specimens were immersed in resin (Eponate 12, Ted Pella, Inc., Redding, CA, USA) overnight and then sliced using the Reichert–Jung Ultracut E ultramicrotome (Reichert, Depew, NY, USA). Additionally, the functional groups on the membrane's surface were assessed using ATR FT-IR spectroscopy. The Nicolet 4700 FT-IR instrument equipped with the multi-reflection Smart Performer® ATR accessory (Thermo Electron, Waltham, MA, USA) was utilized for this analysis. The hydrophilicity of the membrane surface was evaluated by measuring the contact angle between a drop of DI water and the membrane surface. This was conducted using a contact angle video system named VCA-2500 XE (AST products, Inc., Billerica, MA, USA), employing the sessile drop technique. Six observations, at least, were taken at different locations, and the reported contact angle value represents the mean of these measurements.

In our previous investigation (Kadhom *et al*. 2017), we employed a cross-flow reverse osmosis system to quantify water flux and salt rejection. The membrane was inserted into a filter holder cell (HP Filter Holder, 47 mm, stainless steel, EMD Millipore, Billerica, MA, USA) and underwent an 8 h testing process. Test conditions included a pressure of 220 psi, a temperature of 25 °C, and a NaCl solution concentration of 2000 ppm. Water flux was determined by measuring the volume of permeate water transported per unit time. Monitoring and quantification of water flux were conducted using the LABVIEW program according to Eq. (1).

$$J = \frac{V}{\mathrm{A}\,.\,\mathrm{t}} \tag{1}$$

The equation expresses the relationship between water flux (J), permeate water volume (V), membrane area (A), and accumulation time (t).

A conductivity meter from HACH Company in Loveland, CO, USA, was utilized to estimate the overall dissolved salts in both the brackish feed and pure discharged water. The NaCl rejection was calculated using Eq. (2).

$$\mathrm{R} = \left(1 - \frac{Cp}{Cf}\right) \times 100 \tag{2}$$

The salt rejection ratio, denoted as R, is determined by the permeate water conductivity (C_p) and the feed conductivity (C_f).

The solubility of the salt is maintained constant by controlling the system's temperature at 25 °C employing a water bath. However, Scheme 1 shows the system used for membrane operation testing (Kadhom Deng 2019b).

3. Results and discussion

3.1 Surface area measurements of Zr-BADS

The surface areas of Zr-BADS-1 and Zr-BADS-2 NPs were found to be 396.1 and 278.6 m^2/g, respectively. Although these measurements indicate significant surface area, they are somewhat lower than previously prepared MOFs, which could be attributed to the aggregation. For our two prepared MOFs, we noticed that Zr-BADS-1, which is made using DMF as a solvent, has a higher surface area than Zr-BADS-2, the one that was prepared utilizing ethanol as a solvent. This could be attributed to DMF's higher dissolving potential, which could form higher crystallinity and porous powder.

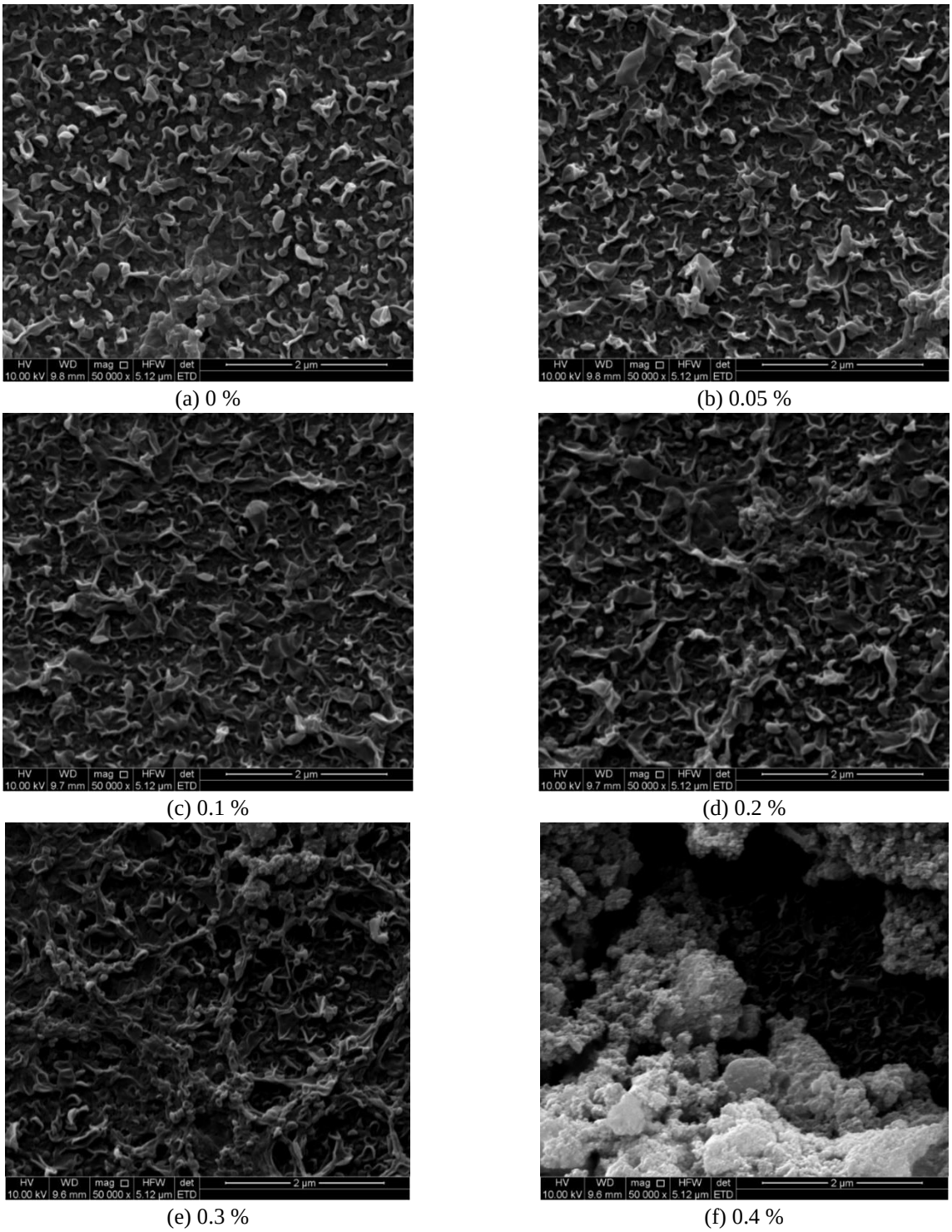

(a) 0 % (b) 0.05 %

(c) 0.1 % (d) 0.2 %

(e) 0.3 % (f) 0.4 %

Fig. 2 SEM images of the TFN membranes filled with Zr-BADS-1: (a) plain TFC membrane, (b) 0.05%, (c) 0.1%, (d) 0.2%, (e) 0.3%, and (f) 0.4%

3.2 SEM characterizations

The morphology of Zr-BADS-embedded TFN membranes was examined using the SEM technique to observe the introduced changes before and after filling; Figs 2 and 3 show the morphology of membranes after filling Zr-BADS-1 and Zr-BADS-2, respectively. Fig. 2a displays the SEM image of the TFC membrane, devoid of additional particles, exhibited a leaf-like morphology characteristic of a standard polyamide layer. Even with the incorporation of Zr-BADS NPs at concentrations up to 0.1%, the leaf-like structure remained largely unaltered. In both figures, it can be noticed that as the ratio of filling particles increases, a change in the membrane's shape is noticed. However, at high filling ratios, aggregation of the particles occurs on the surface. Higher filling ratios led to higher aggregation and eventually decreased the total performance.

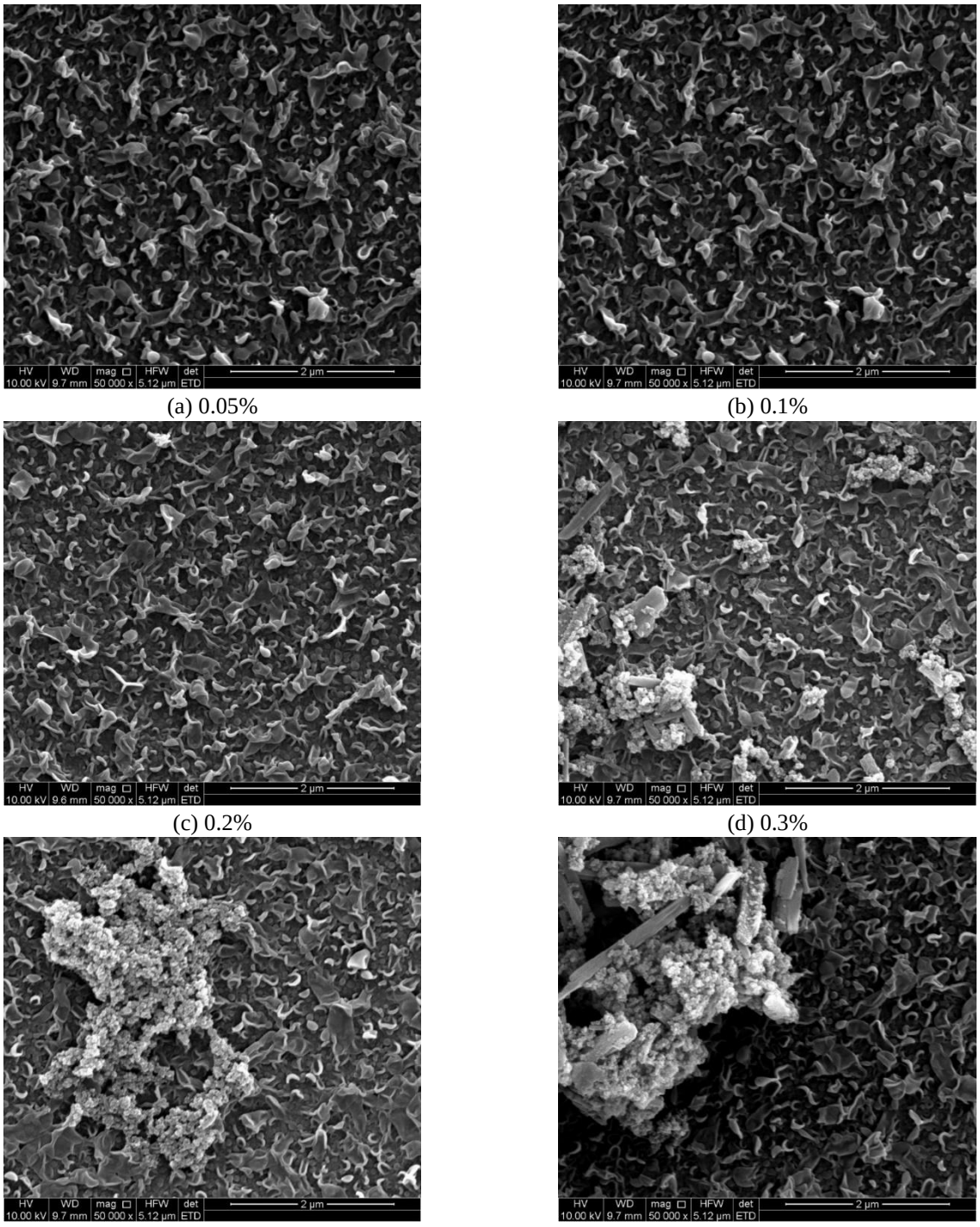

(a) 0.05% (b) 0.1%

(c) 0.2% (d) 0.3%

(e) 0.4% (f) 0.5%

Fig. 3 SEM images of the TFN membranes filled with Zr-BADS-2: (a) 0.05%, (b) 0.1%, (c) 0.2%, (d) 0.3%, (e) 0.4%, and (f) 0.5%

From these images, the particle size of both MOFs was found to be ≤ 100 nm, allowing easy filling within the TFN membrane, whose thickness usually ranges from 100-300 nm (Kalash *et al*. 2020).

3.3 TEM characterizations

Figs. 4a-c show TEM cross-sectional images of the whole membrane, the TFC membrane, and the 0.4% Zr- BADS-filled TFN membrane, respectively. In Fig. 4a, the TFC membrane on the PSU layer is shown, with a thickness of approximately 100 µm. As mentioned in Section 2.3, the support layer was initially cast at 130 µm. Still, its reduced thickness in this image could be attributed to solvent loss and layer shrinkage during phase inversion (Kadhom and Deng 2019a). In Fig. 4b, the cross-sectional perspective of the TFC membrane is illustrated, where the film thickness is around 100-300 nm, which is consistent with the literature

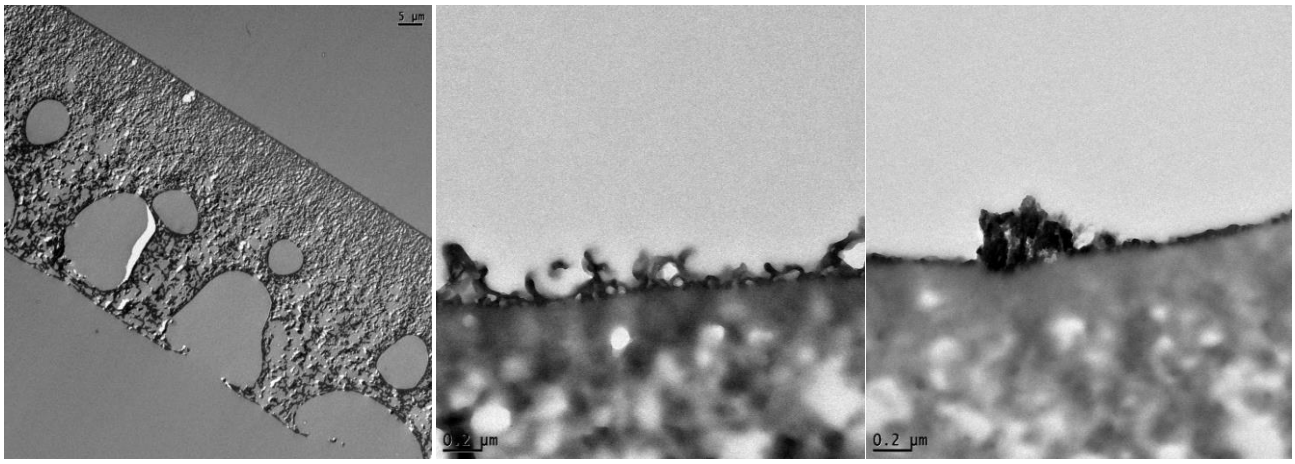

(a) (b) (c)

Fig. 4 TEM cross-sectional images of (a) TFN membrane on PSU support layer, (b) TFC membrane, and (c) TFN membrane filled with Zr-BADS-1

(Kadhom and Deng 2019b). Finally, Fig. 4c illustrates a cross-sectional view of the TFN membrane with an optimal Zr-BADS NPs loading of 0.4%. The TEM analysis revealed densely packed particles within the membranes, forming dark clusters. The Zr-BADS-1 NPs displayed a high level of uniformity within the membrane and influenced its texture.

3.4 FTIR characterization

Surface attenuated total reflection Fourier-transform infrared (ATR FTIR) spectra were acquired from various membrane materials. Figs. 5a and b illustrate the spectra of the TFC membrane on the PSU supporting film and the TFN membranes containing Zr-BADS-1 and Zr-BADS-2 NPs, respectively. The spectrum characteristics of the PSU sheet and TFC membrane chemical groups are mirrored in the spectra of TFN membranes, where peaks corresponding to MOFs are also evident. As the NP fraction increases, the reflected spectra typically observe additional peaks associated with the embedded materials. Analysis of the PSU spectra revealed two prominent peaks at 1150 and 1245 cm^{-1}, attributed to the symmetric stretching of the sulfone group (O=S=O) and the asymmetric stretching of the aryl ethyl group (C–O–C), respectively (Deng *et al*. 2011). Peaks around 1300 and 1325 cm^{-1} suggest asymmetric stretching of the O=S=O sulfone group, while peaks around 1490 and 1590 cm^{-1} indicate stretching of aromatic C–C bonds (Tarboush *et al*. 2008). The introduction of a polyamide thin film layer led to the appearance of peaks at 1350 and 1610 cm^{-1}, attributed to N–H deformation (amide III) and C=O (carboxylic) vibrations, respectively (Lee *et al*. 2008).

Additionally, bending of N–H bonds and stretching of C–The peak indicates N bonds observed around 1545 cm^{-1} (referred to as amide II), while vibration at 1660 cm^{-1} is attributed to stretching of the C=O bond in the amide I region (Shawky *et al*. 2011).

By adding Zr-BADS, no noticeable peaks appear at low loading ratios; yet, at the highest loading ratios, some changes in the spectra are detected. The distinctive peaks observed at around 1650 and 1450 cm^{-1} are attributed to the carboxylate group's in-phase and out-of-phase stretching modes. Specifically, the peak at 1650 cm^{-1} corresponds to the C–C bond in the aromatic molecule of the organic linker, while the peak at 1450 cm^{-1} is attributed to the C–O bond in the carboxylic acid's C–OH group (Zati-Hanani *et al*. 2011). The peak at 680 cm^{-1} corresponds to the O–H bending mode and the peak at 780 cm^{-1} corresponds to the Zr–O mode (Jin and Yang 2017). Additionally, peaks in the area 540 cm^{-1} and 560 cm^{-1} refer to the symmetric and asymmetric stretching of Zr–(OC) (Valenzano *et al*. 2011).

3.5 Contact angle measurements

Fig. 6 illustrates the contact angles measured between a DI water drop and the membrane surface. The inclusion of Zr-BADS NPs led to a higher degree of decrease in the contact angle than in conventional materials, such as hydrophilic silica (Kalash *et al*. 2020). This reduction can be attributed to the hydrophilic nature of the prepared MOFs, although they comprise organic parts within their structure. As depicted in the Fig., Zr-BADS-1 demonstrated a slightly higher degree of hydrophilicity compared to Zr-BADS-2. This discrepancy may stem from the presence of a higher number of surface hydrophilic groups coming from the used solvent, DMF. In fact, DMF is a higher polar aprotic solvent than ethanol, which may retain residuals and have uncoordinated carboxylate groups that contribute to the hydrophilic nature (Israr *et al*. 2016). The second reason is the possibility of producing formic acid via DMF hydrolyzing, which could enhance the hydrophilicity (Cottineau *et al*. 2011). The last probable reason is DMF facilitates the formation of highly crystalline structures with larger pores (Ratajczyk *et al*. 2019), which can enhance water uptake capacity and, therefore, hydrophilicity.

3.6 Performance calculations

Figs. 7a and 7b present the salt rejection and water flux of membranes treated with Zr-BADS-1 and Zr-BADS-2,

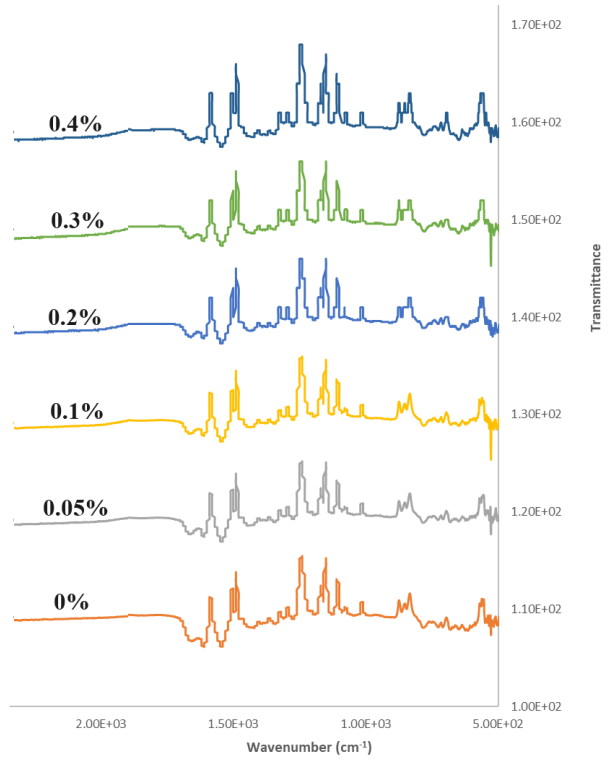

(a)

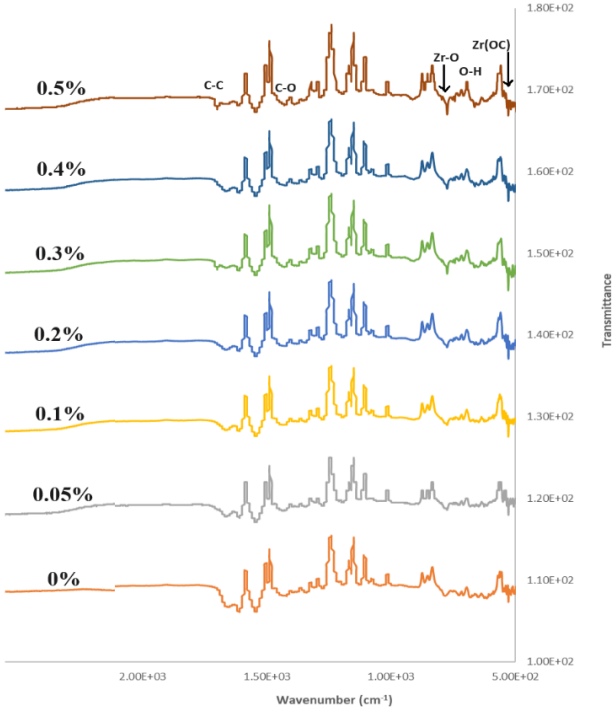

(b)

Fig. 5 ATR FTIR spectra of (a) Zr-BADS-1 and (b) Zr-BADS-2 filled TFN membranes

respectively. For Zr-BADS-1, the optimal addition was found to be 0.3%, resulting in increased permeate water flux from 63.04 L/m^2 h to 81.89 L/m^2 h. However, a marginal reduction was noticed when the salt rejection was

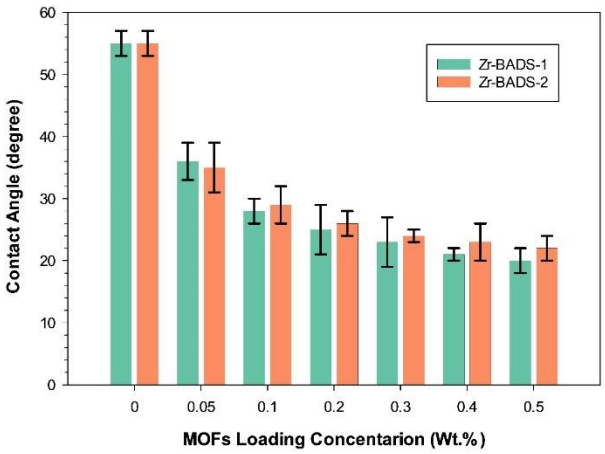

Fig. 6 Contact angle test for the TFC and TFN membranes filled with Zr-BADS

measured, where it changed from 97.49 % to 95.39% when 0.3% was uploaded within the membrane. As depicted in Fig. 7a, incorporating Zr-BADS-1 initially decreased NaCl rejection at low concentrations, but higher NP concentrations improved salt rejection. This initial reduction in rejection is likely related to the provided porosity by Zr-BADS-1, which led to passing the salty water (Cavka *et al*. 2008). However, at higher loading ratios, the charge of the particles could dominate and result in repulsion for the salt ions, knowing that the zeta potential value of Zr.BADS-1 was -20.77 mV. It is worth mentioning that the size of water molecules is around 2.8 Å, which is smaller than that of hydrated ions of the salt (Na^+ = 7.16 Å and Cl^- = 6.64 Å) (Nightingale 1959). Yet, excessive NP loading reduced the water flux due to the aggregation on the TFN membrane surface. Conversely, the increase in water flux by adding NPs peaked at 0.3%, attributed to the hydrophilic nature of zirconium within the structure of Zr-BADS-1 (Furukawa *et al*. 2014). Water flux decreased when the percentage exceeded 0.3%, likely due to NPs agglomeration. Here, the aggregation of particles might hinder water transfer through the membrane by generating a hinder layer, thereby reducing water flux (Wu *et al*. 2021).

Fig. 7b demonstrates the effect of incorporating Zr-BADS-2 NPs into the TFN membrane. As the nanoparticle loading increases, there is a corresponding increase in water flux. For example, by filling 0.3%, the permeate water flux enhanced from 63.04 to 69.45 L/m^2 h, but the salt rejection was negligibly reduced (97.49% vs. 96.36%). The higher loading ratios showed almost stable outcomes. However, with the addition of 0.4% NPs, there was an increase in salt rejection and water flux to 97.55% and 70.04 L/m^2 h, respectively. Zr-BADS-2 could increase the water paths for the water molecules while rejecting the ions due to the Donnan effect (Xiao *et al*. 2021). Further increase in the dose led to a remarkable decrease in salt rejection (data are not shown). We like to mention that each result was performed at least three times to obtain the average and calculate the standard deviation.

The table below compares Zr-BADS performance results with other types of MOFs at their best filling ratios

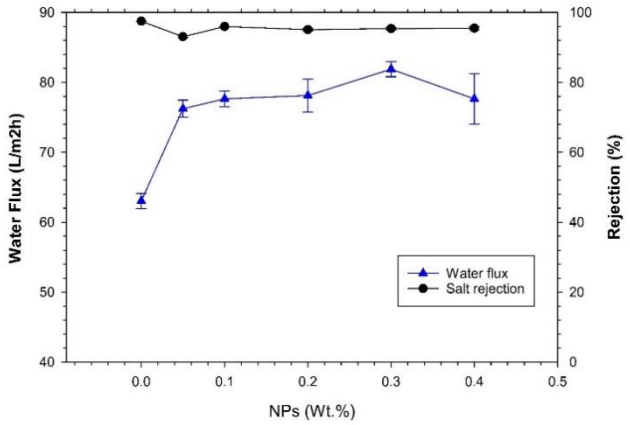

(a)

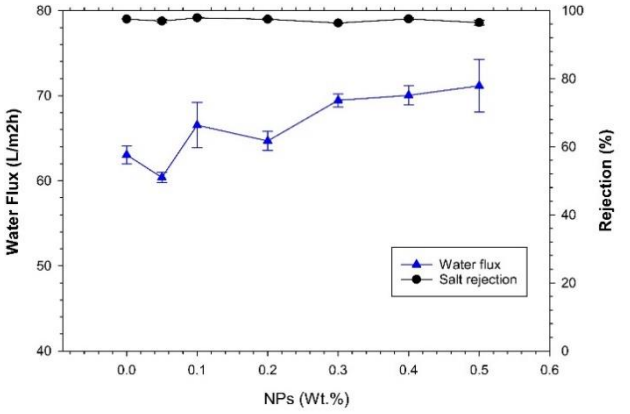

(b)

Fig. 7 Performance results of (a) Zr-BADS-1 and (b) Zr-BADS-2

in RO. From the table, Zr-BADS-1 could be considered one of the best fillers that led to obtaining superior membranes. This could be attributed to its long chain linker, compared to the terephthalic acid of the UiO-66, which could give larger crystallinity units and enhanced porosity. Therefore, water molecules' transfer is facilitated within the MOF. However, Zr-BADS-1's salt rejection is slightly lower than others, which could be attributed to the same reason as the ions could move in higher amounts in wider porosity.

We like to mention that although the surface area of Zr-BADS is lower than many synthesized MOFs, they showed high results. This disparity results from the distinct structural characteristics of Zr-BADS than those of some previously prepared MOFs, such as ZIF-8 or MIL-101; this disparity results from Zr-BADS's distinct structural characteristics. The bicinchoninic acid disodium salt linker employed in Zr-BADS synthesis could create a denser framework with reduced accessible micropores, leading to a diminished overall surface area. The solvothermal synthesis conditions, utilizing dimethylformamide or ethanol as solvents, may affect the pore size distribution and crystallinity, thereby impacting the measured surface area. For reverse osmosis applications, the moderate surface area, combined with the distinct pore architecture, facilitates efficient water transport while reducing the risk of excessive pore flooding that may compromise salt rejection.

Table 1 A performance comparison between Zr-BADS and other fillers

Filler type	Salt rejection (%)	Water flux (L/m^2 h bar)	Reference
Zr-BADS-1	95.39	5.40	This work
Zr-BADS-2	97.36	4.62	This work
Ni-MOFs	99.2	2.50	(Liu *et al*. 2022)
ZIF-8	99.5	3.35	(Duan *et al*. 2015)
ZIF-8/CNT	99.21	3.60	(Lee *et al*. 2020)
UiO-66	99.35	3.67	(Liu *et al*. 2019)
ZIF-67	99.28	2.94	(Zhao *et al*. 2021)
Defective ZIF-8	98.6	2.61	(Zhao *et al*. 2021)
MIL-125	98.6	4.11	(Kadhom *et al*. 2017)
UiO-66	98.8	3.62	(Kadhom *et al*. 2017)

3.7 MOFs mechanisms in TFN membrane

Our experimental results, in addition to other groups' observations, show that MOFs present remarkable fillers for the TFN membrane. The following points show the ways of MOFs incorporation.

1. Enhanced Selectivity: The adaptable pore dimensions and surface properties of MOFs offer precise control over the molecular sieving attributes of TFN membranes. Through meticulous selection of MOFs with specific pore sizes and functional groups, it becomes possible to fabricate membranes capable of allowing the passage of water molecules while effectively inhibiting the transport of ions, organic compounds, and other contaminants (Kadhom *et al*. 2017). This capacity for selectivity is indispensable for attaining high water purity levels in reverse osmosis processes.

2. Increased Permeability: MOFs' very high (commonly) surface area and interconnected porous structures facilitate rapid and effective transport of water molecules within the membrane. This is advantageous for boosting water flux rates in TFN membranes by reducing resistance to water flux by providing channels within the membrane. Additionally, the hydrophilic nature (which is required for this type of application) of many MOFs promotes water adsorption and transport (Kadhom *et al*. 2023).

3. Improved Stability: Incorporating MOFs into TFN membranes can enhance their mechanical and chemical stability by serving as reinforcing fillers within the membrane matrix (Kadhom and Deng 2019b). Strong coordination interactions between metal ions and organic ligands in MOFs allow membranes to tolerate rigorous working conditions without deformation or degradation. MOFs might also protect membranes against fouling, oxidative damage, and other environmental issues (Firouzjaei *et al*. 2020).

4. Customization of Surface Properties: MOFs offer a versatile platform for integrating diverse chemical groups, such as hydrophilic or hydrophobic moieties, metal complexes, or reactive sites. This flexibility enables precise tuning of TFN membranes to enhance their surface properties and interactions, leading to tailored performance

characteristics (Kitao *et al*. 2017). Functionalized MOFs can augment membrane hydrophilicity to mitigate fouling or enhance antibacterial properties to bolster resistance against biofouling.

5. Tailored Attributes: Strategic design may precisely customize MOF attributes because of their modularity. By selecting metal ions, organic ligands, and synthesis parameters, pore size, shape, surface area, chemical stability, and surface chemistry may be controlled. These properties may be carefully modified for reverse osmosis applications, such as saltwater desalination (Shen *et al*. 2021).

4. Conclusions

This study presents a systematic investigation into the synthesis, characterization, and performance evaluation of TFN membranes embedded with zirconium-based MOFs for RO applications. The successful synthesis of Zr-BADS-1 and Zr-BADS-2 MOFs was achieved via a solvothermal method, demonstrating high surface area and potential for effective water permeation. Morphological analysis revealed uniform distribution and dense packing of Zr-BADS NPs within the TFN membranes, influencing their texture and enhancing performance. FTIR spectroscopy confirmed the presence of characteristic MOF peaks within the membranes, with changes observed at higher loading ratios. Performance evaluation demonstrated improved water flux with the addition of Zr-BADS-1 NPs, reaching a peak at 0.3% loading, while salt rejection exhibited a complex interplay between porosity and charge effects. Comparative analysis with other MOFs highlighted the superior performance of Zr-BADS-1 in terms of salt rejection and water flux, positioning it as a promising filler for RO membranes. Future work could consider the synthesis of pure Zr-BADS membranes on support layers and investigate their performance in the NF, RO, and FO applications. Here, the findings of our work offer a base on which to step forward in Zr-BADS applications in research and large-scale industries.

Acknowledgments

The authors like to thank their affiliations for partially supporting this project.

References

Alalwan, H.A., Kadhom, M.A. and Alminshid, A.H. (2020), "Removal of heavy metals from wastewater using agricultural byproducts", *J. Water Suppl. Res. Technol. Aqua*, **69**(2), 99-112. https://doi.org/10.2166/aqua.2020.133

Albayati, N., AL-dulaimy, W.Y.M., Jweeg, M.J., Kadhom, M., Salih, S. and Abdullah, G. (2024), "Synthesis and characterisation of novel metal-organic frameworks (MOFs) based on zirconium and bicinchoninic acid", *Curr. Chem. Lett.*, **13**(1), 41-48. https://doi.org/10.5267/j.ccl.2023.9.001

Albayati, N. and Kadhom, M. (2020), "Preparation of functionalised UiO-66 metal-organic frameworks (MOFs) nanoparticles using deep eutectic solvents as a benign medium", *Micro Nano Lett.*, **15**(15), 1075-1078. https://doi.org/10.1049/mnl.2020.0360

Al-Furaiji, M., Kadhom, M., Kalash, K., Waisi, B. and Albayati, N. (2020), "Preparation of thin-film composite membranes supported with electrospun nanofibers for desalination by forward osmosis", *Drink. Water Eng. Sci.*, **13**(2), 51-57. https://doi.org/10.5194/dwes-13-51-2020

Al-Furaiji, M., Waisi, B., Kalash, K. and Kadhom, M. (2022), "Effect of polymer substrate on the performance of thin-film composite nanofiltration membranes", *Int. J. Polym. Anal. Charact.*, **27**(5), 316-325. https://doi.org/10.1080/1023666X.2022.2073008

Allendorf, M.D., Bauer, C.A., Bhakta, R.K. and Houk, R.J.T. (2009), "Luminescent metal-organic frameworks", *Chem. Soc. Rev.*, **38**(5), 1330. https://doi.org/10.1039/b802352m

An, J. and Rosi, N.L. (2010), "Tuning MOF CO_2 adsorption properties via cation exchange", *J. Am. Chem. Soc.*, **132**(16), 5578-5579. https://doi.org/10.1021/ja1012992

Azeez, N.R., Salih, S.S., Kadhom, M., Mohammed, H.N. and Ghosh, T.K. (2023), "Enhanced termination of zinc and cadmium ions from wastewater employing plain and chitosan-modified mxenes: Synthesis, characterization, and adsorption performance", *Green Chem. Eng.*, **5**(3), 339-347. https://doi.org/10.1016/j.gce.2023.08.003

Cavka, J.H., Jakobsen, S., Olsbye, U., Guillou, N., Lamberti, C., Bordiga, S. and Lillerud, K.P. (2008), "A new zirconium inorganic building brick forming metal organic frameworks with exceptional stability", *J. Am. Chem. Soc.*, **130**(42), 13850-13851. https://doi.org/10.1021/ja8057953

Cottineau, T., Richard-Plouet, M., Mevellec, J.Y. and Brohan, L. (2011), "Hydrolysis and complexation of N , N -dimethylformamide in new nanostructurated titanium oxide hybrid organic-inorganic sols and gel", *J. Phys. Chem. C*, **115**(25), 12269-12274. https://doi.org/10.1021/jp201864g

Della Rocca, J., Liu, D. and Lin, W. (2011), "Nanoscale metal-organic frameworks for biomedical imaging and drug delivery", *Accounts Chem. Res.*, **44**(10), 957-968. https://doi.org/10.1021/ar200028a

Deng, H., Xu, Y., Chen, Q., Wei, X. and Zhu, B. (2011), "High flux positively charged nanofiltration membranes prepared by UV-initiated graft polymerization of methacrylatoethyl trimethyl ammonium chloride (DMC) onto polysulfone membranes", *J. Membr. Sci.*, **366**(1-2), 363-372. https://doi.org/10.1016/j.memsci.2010.10.029

Duan, J., Pan, Y., Pacheco, F., Litwiller, E., Lai, Z. and Pinnau, I. (2015), "High-performance polyamide thin-film-nanocomposite reverse osmosis membranes containing hydrophobic zeolitic imidazolate framework-8", J. Membr. Sci., **476**, 303-310. https://doi.org/10.1016/j.memsci.2014.11.038

Elimelech, M. and Phillip, W.A. (2011), "The future of seawater desalination: energy, technology, and the environment", *Science*, **333**(6043), 712-717. https://doi.org/10.1126/science.1200488

Farahbakhsh, J., Najafi, M., Golgoli, M., Haeri, S.Z., Khiadani, M., Razmjou, A. and Zargar, M. (2024), "Dual modification of reverse osmosis membranes with NH2-MIL-125 and functionalised multiwalled carbon nanotubes for enhanced nanoplastic removal", *Chemosphere*, **361**, 142401. https://doi.org/10.1016/j.chemosphere.2024.142401

Farha, O.K., Eryazici, I., Jeong, N.C., Hauser, B.G., Wilmer, C.E., Sarjeant, A.A., Snurr, R.Q., Nguyen, S.T., Yazaydın, A.Ö. and Hupp, J.T. (2012), "Metal-organic framework materials with ultrahigh surface areas: Is the sky the limit?", *J. Am. Chem. Soc.*, **134**(36), 15016-15021. https://doi.org/10.1021/ja3055639

Firouzjaei, M.D., Seyedpour, S.F., Aktij, S.A., Giagnorio, M., Bazrafshan, N., Mollahosseini, A., Samadi, F., Ahmadalipour, S., Firouzjaei, F.D., Esfahani, M.R., Tiraferri, A., Elliott, M., Sangermano, M., Abdelrasoul, A., McCutcheon, J.R., Sadrzadeh, M., Esfahani, A.R. and Rahimpour, A. (2020), "Recent advances

in functionalized polymer membranes for biofouling control and mitigation in forward osmosis", *J. Membr. Sci.*, **596**, 117604. https://doi.org/10.1016/j.memsci.2019.117604

Furukawa, H., Gándara, F., Zhang, Y.B., Jiang, J., Queen, W.L., Hudson, M.R. and Yaghi, O.M. (2014), "Water adsorption in porous metal-organic frameworks and related materials", *J. Am. Chem. Soc.*, **136**(11), 4369-4381. https://doi.org/10.1021/ja500330a

Hua, B., Xiong, H., Kadhom, M., Wang, L., Zhu, G., Yang, J., Cunningham, G. and Deng, B. (2017), "Physico-Chemical Processes", *Water Environ. Res.*, **89**(10), 974-1028. https://doi.org/10.2175/106143017X15023776270214

Israr, F., Chun, D., Kim, Y. and Kim, D.K. (2016), "High yield synthesis of Ni-BTC metal-organic framework with ultrasonic irradiation: Role of polar aprotic DMF solvent", *Ultrasonics Sonochem.*, **31**, 93-101. https://doi.org/10.1016/j.ultsonch.2015.12.007

Jin, Z. and Yang, H. (2017), "Exploration of Zr-metal-organic framework as efficient photocatalyst for hydrogen production", *Nanosc. Res. Lett.*, **12**(1), 539. https://doi.org/10.1186/s11671-017-2311-6

Kadhom, M. (2023a), "A review on the polyamide thin film composite (TFC) membrane used for desalination: Improvement methods, current alternatives, and challenges", *Chem. Eng. Res. Des.*, **191**, 472-492. https://doi.org/10.1016/j.cherd.2023.02.002

Kadhom, M. (2023b), "MXenes in membrane-based water treatment applications", *Age of MXenes*, **4**, 121-139. https://doi.org/10.1021/bk-2023-1445.ch006

Kadhom, M., Albayati, N., Alalwan, H. and Al-Furaiji, M. (2020), "Removal of dyes by agricultural waste", *Sust. Chem. Pharm.*, **16**, 100259. https://doi.org/10.1016/j.scp.2020.100259

Kadhom, M., Albayati, N., Salih, S., Al-Furaiji, M., Bayati, M. and Deng, B. (2019), "Role of cellulose micro and nano crystals in thin film and support layer of nanocomposite membranes for brackish water desalination", *Membranes*, **9**(8), 101. https://doi.org/10.3390/membranes9080101

Kadhom, M., Al-Furaiji, M., Salih, S., Al-Obaidi, M.A., Abdullah, G.H. and Albayati, N. (2023), "A review on UiO-66 applications in membrane-based water treatment processes", *J. Water Proc. Eng.*, **51**, 103402. https://doi.org/10.1016/j.jwpe.2022.103402

Kadhom, M. and Deng, B. (2018), "Metal-organic frameworks (MOFs) in water filtration membranes for desalination and other applications", *Appl. Mater. Today*, **11**, 219-230. https://doi.org/10.1016/j.apmt.2018.02.008

Kadhom, M. and Deng, B. (2019a), "Synthesis of high-performance thin film composite (TFC) membranes by controlling the preparation conditions: Technical notes", *J. Water Proc. Eng.*, **30**, 100542. https://doi.org/10.1016/j.jwpe.2017.12.011

Kadhom, M. and Deng, B. (2019b), "Thin film nanocomposite membranes filled with bentonite nanoparticles for brackish water desalination: A novel water uptake concept", *Micropor. Mesopor. Mater.*, **279**, 82-91. https://doi.org/10.1016/j.micromeso.2018.12.020

Kadhom, M., Hu, W. and Deng, B. (2017), "Thin film nanocomposite membrane filled with metal-organic frameworks uio-66 and mil-125 nanoparticles for water desalination", *Membranes*, **7**(2), 31. https://doi.org/10.3390/membranes7020031

Kadhom, M., Kalash, K. and Al-Furaiji, M. (2022), "Performance of 2D MXene as an adsorbent for malachite green removal", *Chemosphere*, **290**, 133256. https://doi.org/10.1016/j.chemosphere.2021.133256

Kalash, K., Kadhom, M. and Al-Furaiji, M. (2020), "Thin film nanocomposite membranes filled with MCM-41 and SBA-15 nanoparticles for brackish water desalination via reverse osmosis", *Environ. Technol. Innov.*, **20**, 101101. https://doi.org/10.1016/j.eti.2020.101101

Kitao, T., Zhang, Y., Kitagawa, S., Wang, B. and Uemura, T. (2017), "Hybridization of MOFs and polymers", *Chem. Soc. Rev.*, **46**(11), 3108-3133. https://doi.org/10.1039/C7CS00041C

Koriem, O.A., Showman, M.S., El-Shazly, A.H. and Elkady, M.F. (2023), "Cellulose acetate/polyvinylidene fluoride based mixed matrix membranes impregnated with UiO-66 nano-MOF for reverse osmosis desalination", *Cellulose*, **30**(1), 413-426. https://doi.org/10.1007/s10570-022-04889-9

Lee, C.Y., Farha, O.K., Hong, B.J., Sarjeant, A.A., Nguyen, S.T. and Hupp, J.T. (2011), "Light-harvesting metal-organic frameworks (MOFs): Efficient strut-to-strut energy transfer in bodipy and porphyrin-based MOFs", *J. Am. Chem. Soc.*, **133**(40), 15858-15861. https://doi.org/10.1021/ja206029a

Lee, H.S., Im, S.J., Kim, J.H., Kim, H.J., Kim, J.P. and Min, B.R. (2008), "Polyamide thin-film nanofiltration membranes containing TiO2 nanoparticles", *Desalination*, **219**(1-3), 48-56. https://doi.org/10.1016/j.desal.2007.06.003

Lee, J.Y., Tang, C.Y. and Huo, F. (2014), "Fabrication of porous matrix membrane (PMM) using metal-organic framework as green template for water treatment", *Sci. Rep.*, **4**(1), 3740. https://doi.org/10.1038/srep03740

Lee, T.H., Roh, J.S., Yoo, S.Y., Roh, J.M., Choi, T.H. and Park, H.B. (2020), "High-performance polyamide thin-film nano-composite membranes containing ZIF-8/CNT hybrid nanofillers for reverse osmosis desalination", *Ind. Eng. Chem. Res.*, **59**(12), 5324-5332. https://doi.org/10.1021/acs.iecr.9b04810

Li, L., Wang, X., Zhang, D., Guo, R. and Du, X. (2015), "Excellent adsorption of ultraviolet filters using silylated MCM-41 mesoporous materials as adsorbent", *Appl. Surf. Sci.*, **328**, 26-33. https://doi.org/10.1016/j.apsusc.2014.11.116

Liu, L., Xie, X., Qi, S., Li, R., Zhang, X., Song, X. and Gao, C. (2019), "Thin film nanocomposite reverse osmosis membrane incorporated with UiO-66 nanoparticles for enhanced boron removal", *J. Membr. Sci.*, **580**, 101-109. https://doi.org/10.1016/j.memsci.2019.02.072

Liu, X., Demir, N.K., Wu, Z. and Li, K. (2015), "Highly water-stable zirconium metal-organic framework UiO-66 membranes supported on alumina hollow fibers for desalination", *J. Am. Chem. Soc.*, **137**(22), 6999-7002. https://doi.org/10.1021/jacs.5b02276

Liu, Y., Ng, Z., Khan, E.A., Jeong, H.K., Ching, C. and Lai, Z. (2009), "Synthesis of continuous MOF-5 membranes on porous α-alumina substrates", Micropor. Mesopor. Mater., **118**(1-3), 296-301. https://doi.org/10.1016/j.micromeso.2008.08.054

Liu, Y., Wang, X., Zong, Z., Lin, R., Zhang, X., Chen, F., Ding, W., Zhang, L., Meng, X. and Hou, J. (2022), "Thin film nano-composite membrane incorporated with 2D-MOF nanosheets for highly efficient reverse osmosis desalination", *J. Membr. Sci.*, **653**, 120520. https://doi.org/10.1016/j.memsci.2022.120520

Ma, L., Abney, C. and Lin, W. (2009), "Enantioselective catalysis with homochiral metal-organic frameworks", *Chem. Soc. Rev.*, **38**(5), 1248. https://doi.org/10.1039/b807083k

Murray, L.J., Dincă, M. and Long, J.R. (2009), "Hydrogen storage in metal-organic frameworks", *Chem. Soc. Rev.*, **38**(5), 1294. https://doi.org/10.1039/b802256a

Nightingale, E.R. (1959), "Phenomenological theory of ion solvation. Effective radii of hydrated ions", *J. Phys. Chem.*, **63**(9), 1381-1387. https://doi.org/10.1021/j150579a011

Oladoye, P.O., Kadhom, M., Khan, I., Hama Aziz, K.H. and Alli, Y.A. (2023), "Advancements in adsorption and photodegradation technologies for Rhodamine B dye wastewater treatment: fundamentals, applications, and future directions", *Green Chem. Eng.*, **5**(4), 440-460. https://doi.org/10.1016/j.gce.2023.12.004

Ratajczyk, P., Sobczak, S. and Katrusiak, A. (2019), "High-pressure structure and properties of N , N -Dimethylformamide (DMF)", *Crystal Growth Des.*, **19**(2), 896-901. https://doi.org/10.1021/acs.cgd.8b01452

Salih, S.S., Kadhom, M., Shihab, M.A. and Ghosh, T.K. (2022), "Competitive adsorption of Pb(II) and phenol onto modified chitosan/vermiculite adsorbents", *J. Polym. Environ.*, **30**(10), 4238-4251. https://doi.org/10.1007/s10924-022-02515-0

Salih, S.S., Mahdi, A., Kadhom, M. and Ghosh, T.K. (2019), "Competitive adsorption of As(III) and As(V) onto chitosan/ diatomaceous earth adsorbent", J. Environ. Chem. Eng., **7**(5), 103407. https://doi.org/10.1016/j.jece.2019.103407

Salih, S.S., Mohammed, H.N., Abdullah, G.H., Kadhom, M. and Ghosh, T.K. (2020), "Simultaneous removal of Cu(II), Cd(II), and industrial dye onto a composite chitosan biosorbent", *J. Polym. Environ.*, **28**(1), 354-365. https://doi.org/10.1007/s10924-019-01612-x

Shawky, H.A., Chae, S.R., Lin, S. and Wiesner, M.R. (2011), "Synthesis and characterization of a carbon nanotube/polymer nanocomposite membrane for water treatment", *Desalination*, **272**(1-3), 46-50. https://doi.org/10.1016/j.desal.2010.12.051

Shen, Y., Pan, T., Wang, L., Ren, Z., Zhang, W. and Huo, F. (2021), "Programmable logic in metal-organic frameworks for catalysis", *Adv. Mater.*, **33**(46). https://doi.org/10.1002/adma.202007442

Tarboush, B.J.A., Rana, D., Matsuura, T., Arafat, H.A. and Narbaitz, R.M. (2008), "Preparation of thin-film-composite polyamide membranes for desalination using novel hydrophilic surface modifying macromolecules", *J. Membr. Sci.*, **325**(1), 166-175. https://doi.org/10.1016/j.memsci.2008.07.037

Valenzano, L., Civalleri, B., Chavan, S., Bordiga, S., Nilsen, M.H., Jakobsen, S., Lillerud, K.P. and Lamberti, C. (2011), "Disclosing the complex structure of UiO-66 metal organic framework: A synergic combination of experiment and theory", *Chem. Mater.*, **23**(7), 1700-1718. https://doi.org/10.1021/cm1022882

Van der Bruggen, B. and Vandecasteele, C. (2002), "Distillation vs. membrane filtration: Overview of process evolutions in seawater desalination", *Desalination*, **143**(3), 207-218. https://doi.org/10.1016/S0011-9164(02)00259-X

Wu, X., Yang, L., Shao, W., Lu, X., Liu, X. and Li, M. (2021), "Fabrication of high performance TFN membrane incorporated with graphene oxide via support-free interfacial polymerization", *Sci. Total Environ.*, **793**, 148503. https://doi.org/10.1016/j.scitotenv.2021.148503

Xiao, F., Hu, X., Chen, Y. and Zhang, Y. (2019), "Porous Zr-Based Metal-Organic Frameworks (Zr-MOFs)-incorporated thin-film nanocomposite membrane toward enhanced desalination performance", *ACS Appl. Mater. Interf.*, **11**(50), 47390-47403. https://doi.org/10.1021/acsami.9b17212

Xiao, S., Huo, X., Tong, Y., Cheng, C., Yu, S. and Tan, X. (2021), "Improvement of thin-film nanocomposite (TFN) membrane performance by CAU-1 with low charge and small size", *Sep. Purif. Technol.*, **274**, 118467. https://doi.org/10.1016/j.seppur.2021.118467

Yaseen, S.M., Salih, S.S., Kadhom, M. and Mohammed, H.N. (2023), "Enhancement of phenol recovery from wastewater by nanofluid utilizing liquid-liquid extraction method in a membrane-based contactor", *Chem. Eng. Res. Des.*, **196**, 404-412. https://doi.org/10.1016/j.cherd.2023.06.064

Yin, J., Kim, E.S., Yang, J. and Deng, B. (2012), "Fabrication of a novel thin-film nanocomposite (TFN) membrane containing MCM-41 silica nanoparticles (NPs) for water purification", *J. Membr. Sci.*, **423-424**, 238-246. https://doi.org/10.1016/j.memsci.2012.08.020

Zati-Hanani, S., Adnan, R., Latip, A.F.A. and Sipaut, C.S. (2011), "Synthesis, characterization and thermal properties of two novel Lanthanide 2,2'-Biquinoline-4,4'-Dicarboxylate Complexes (Sintesis, Pencirian dan Sifat Terma Dua Kompleks Lantanida 2,2'-bikuinolin-4,4'-dikarboksilat)", *Sains Malaysiana*, **40**(9).

Zhao, D.L., Yeung, W.S., Zhao, Q. and Chung, T.S. (2020), "Thin-film nanocomposite membranes incorporated with UiO-66-NH2 nanoparticles for brackish water and seawater desalination", *J. Membr. Sci.*, **604**, 118039. https://doi.org/10.1016/j.memsci.2020.118039

Zhao, L., Chang, P.C.Y. and Ho, W.S.W. (2013), "High-flux reverse osmosis membranes incorporated with hydrophilic additives for brackish water desalination", *Desalination*, **308**, 225-232. https://doi.org/10.1016/j.desal.2012.07.020

Zhao, Q., Zhao, D.L. and Chung, T.S. (2021), "Thin-film nanocomposite membranes incorporated with defective ZIF-8 nanoparticles for brackish water and seawater desalination", *J. Membr. Sci.*, **625**, 119158. https://doi.org/10.1016/j.memsci.2021.119158

Zhao, Q., Zhao, D.L., Nai, M.H., Chen, S.B. and Chung, T.S. (2021), "Nanovoid-enhanced thin-film composite reverse osmosis membranes using ZIF-67 nanoparticles as a sacrificial template", *ACS Appl. Mater. Interf.*, **13**(28), 33024-33033. https://doi.org/10.1021/acsami.1c07673

CC